http://dx.doi.org/10.6113/TKPE.2013.18.1.26

전기자동차용 리튬이온 배터리 급속충전장치 설계와 제어

강태원[1], 서용석†, 박현철[2], 강병익[2], 김성훈[2]

A Design and Control of Rapid Electric Vehicle Charging System for Lithium-Ion Battery

Taewon Kang[1], Yongsug Suh†, Hyeoncheol Park[2], Byungik Kang[2], and Simon Kim[2]

Abstract - This paper presents a simple and cost-effective stand-alone rapid battery charging system of 30kW for electric vehicles. The proposed system mainly consists of active front-end rectifier of neutral point clamped 3-level type and non-isolated bi-directional dc-dc converter of multi-phase interleaved half-bridge topology. The charging system is designed to operate for both lithium-polymer and lithium-ion batteries. The complete charging sequence is made up of three sub-interval operating modes; pre-charge mode, constant-current mode, and constant-voltage mode. The pre-charge mode employs the stair-case shaped current profile to accomplish shorter charging time while maintaining the reliable operation of the battery. The proposed system is specified to reach the full-charge state within less than 16min for the battery capacity of 8kWh by supplying the charging current of 78A. Owing to the simple and compact power conversion scheme, the proposed solution has superior module-friendly mechanical structure which is absolutely required to realize flexible power expansion capability in a very high-current rapid charging system.

Keywords: EV, PHEV, bi-directional DC-DC converter, rapid charging system, li-ion polymer battery

1. Introduction

Plug-in Hybrid Electric Vehicle (PHEV) is becoming an attractive alternative to internal combustion engine vehicles in modern transportation industry. One way to achieve the practical all-electric cruising range of electric vehicles is to implement well distributed fast charger infrastructure. Such a structure would provide greater mobility for the PHEV user, since during short stops the PHEV batteries could be charged from typically 20 to 80% of nominal charge. These fast chargers will be installed in highway rest areas and convenient city refueling points. The newly developed dc fast chargers support very fast charging sequences even for heavy vehicles [1]-[4].

There has been growing attention on the various kinds of PHEV rapid charging system in PHEV related industry. The on-board type charger would be appropriate for night time charging from a household utility outlet, or for charging during daytime at work places or malls. On-board chargers are the preferred choice of customers due to its usage simplicity, but the problem is that high power level is difficult to achieve because of its weight, space, and total cost [5][6]. Off-board stand-alone rapid charger installed in a separate off-line charging station is regarded to be one of many practical approaches to solve the limitation of on-board chargers. The off-board charger can be compared to a gas station used for an internal combustion engine vehicle, thus it is aimed at rapid charging. As compared to on-board charger installed inside the PHEV, off-board rapid charger is not critically limited by the weight and volume requirement. With advancement of battery technology, the desire of more on-board battery capacity for more all-electric range and less gasoline consumption is evident for PHEV's or EV's. Therefore there is a trend for battery chargers shifting from compact low

Paper number: TKPE-2013-18-1-4 ISSN: 1229-2214
† Corresponding author: ysuh@jbnu.ac.kr, Electrical Engineering, Chonbuk Nat'l. University
Tel: +82-63-270-3381 Fax: +82-63-270-2394
[1] Electrical Engineering, Chonbuk Nat'l. University
[2] Iljin Electric Co., Ltd.
Manuscript received Oct. 25, 2012; accepted Nov. 25, 2012
— 본 논문은 2012년 전력전자학술대회 외부장학금 수혜논문임

power on-board installation to shared large high-power off-board charging station [7].

In most of charger systems for electric vehicles, bi-directional converters for charging and discharging the batteries are required. The bi-directional converter may be transformer-isolated or non-isolated, depending on the application [8]. Galvanic isolation by a transformer provides a measure of safety, and the design of this transformer introduces many choices. Operating the transformer at high frequencies can increase power density and decrease material cost. This requires a low to high frequency converter on the primary side, a high frequency to dc converter on the secondary side, and a transformer with low leakage inductance and proximity effect losses in between [9][10]. Therefore, galvanic isolation by high-frequency transformer results in more device counts for power converters and a snubber circuitry to deal with the energy trapped in leakage inductance of transformer. As compared to high-frequency transformer-isolated bi-directional dc-dc converters, non-isolated bi-directional dc-dc converters generally have advantages of simple structure, high efficiency, low cost, high reliability, etc. Several non-isolated bi-directional dc-dc converters have been reported in previous literatures [11]-[14].

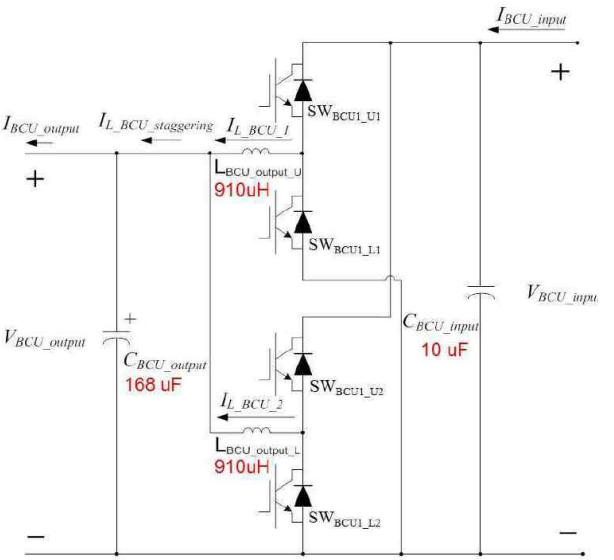

Fig. 2 Bi-directional DC-DC converter used in Battery Charging Unit(BCU)

This paper presents a simple and cost-effective rapid battery charging system for electric vehicles. The rapid battery charging system is implemented in a separate stand-alone off-line charging station located outside of electric vehicle. The proposed charging system mainly consists of active front-end rectifier of neutral point clamped 3-level type and non-isolated bi-directional dc-dc converter of multi-phase interleaved half-bridge topology. Interleaved half-bridge dc-dc converters adopt a coupled output inductor to reduce the size of current ripple or size of core. The charging system is designed to operate for both lithium-polymer and lithium-ion batteries. The control algorithm for the proposed system is set to meet the long life-cycle and safe operating requirement of both type of battery. The complete power converter system can deal with bi-directional power flow between the ac grid and energy storage devices. The discharging operation mode of energy storage device can be effectively utilized for feeding the stored energy back

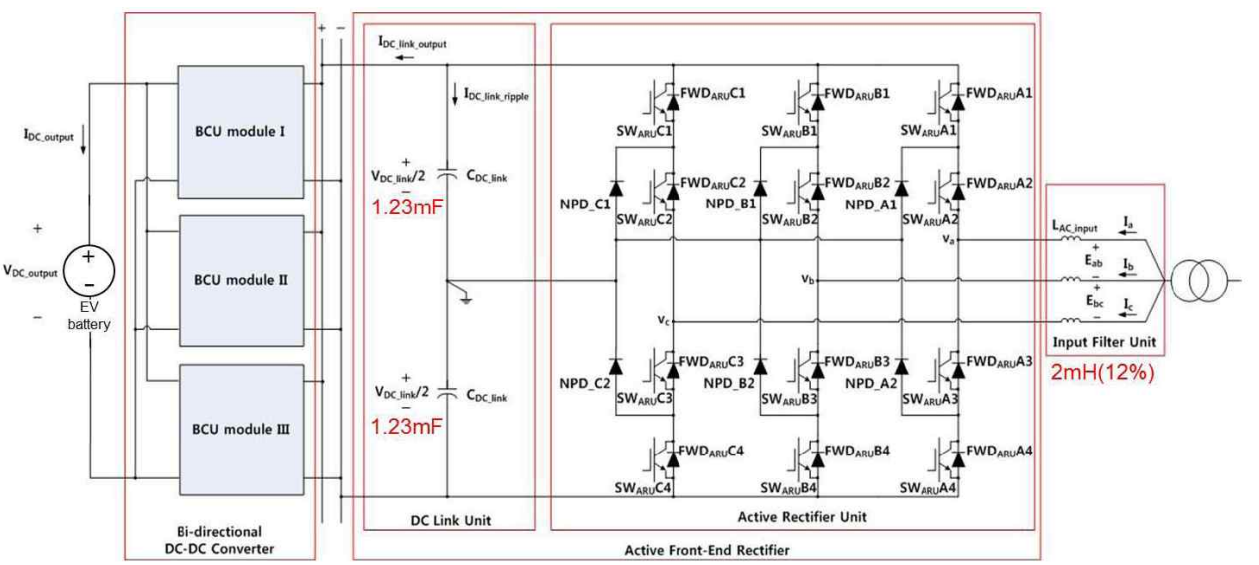

Fig. 1 Proposed battery charging and discharging inverter system

to local grid by PHEV in smart grid concept, i.e. Vehicle to Grid (V2G) operation or ancillary service within micro-grid.

The proposed charging system in this paper is equipped with a line-frequency transformer for galvanic isolation at the ac input side of system. Despite of its weight and volume, this low-frequency transformer has the cutting-edge advantage of low cost and simple interface in a separate off-line charging station. The power converter topology proposed in this paper has less number of power switches as compared to those of state-of-the-art solutions employing isolated bi-directional dc-dc converters, particularly for on-board chargers. Owing to the simple and compact power conversion scheme, the proposed solution has superior module-friendly mechanical structure which is absolutely required to realize flexible power expansion capability in a very high-current rapid charging system. This paper is organized as follows. Section II describes the design of active front-end rectifier and non-isolated bi-directional dc-dc converter in the rapid charging system. Design of coupled inductor is presented in Section III. Proposed control algorithm of lithium-ion polymer battery charging system is explained in Section IV. Simulation and experimental result on a 30kW rapid charging system are provided in Section V and Section VI draws the conclusion.

2. Design of Active Front-end Rectifier and Non-isolated Bi-directional DC-DC Converter

Figure 1 shows the schematic of rapid charger system proposed in this paper. Overall battery charging and discharging system consists of active front-end rectifier of neutral point clamped 3-level type and non-isolated bi-directional dc-dc converter of multi-phase interleaved half-bridge topology. Owing to the high effective switching frequency of 3-level active front-end rectifier, the leakage inductance of transformer can be effectively utilized as the ac input filter inductance. The Active Rectifier Unit (ARU) regulates the dc link voltage at the nominal value of 858V. The control algorithm of ARU is equipped with both positive and negative sequence ac input current regulating loop of dq-synchronous frames, thereby being able to deal with unbalanced ac input supply [15]. The dc link capacitor in DC Link Unit (DLU) is designed to meet the energy factor of 5J/kVA. In rapid charger systems, bi-directional dc-dc converter plays a significant role both in system performance and cost. The Battery Charging Unit (BCU) in the proposed system consists of multiple non-isolated bi-directional dc-dc converter modules. The basic building blocks of two-phase interleaved half-bridge topology are connected in parallel depending on the system requirement of charging/discharging capacity.

In this paper, three modules are employed to realize the maximum charging current of 78A. The power converter topology proposed in this paper has less number of power switches as compared to those of state-of-the-art solutions employing isolated bi-directional dc-dc converters, particularly for on-board chargers. As shown in Fig. 2 power can flow in both directions within BCU, thus coping with charging and discharging mode of battery; buck-operation mode and boost-operation mode. When the energy flows from grid to the vehicle (G2V), it operates under buck-operation mode to charge the battery in electric vehicles; upper switches in half-bridge are controlled to regulate the output. When the energy flows from vehicle to the grid (V2G), it operates under boost-operation mode; lower switches are controlled to regulate the output power into the dc link. In this boost-operation mode, electric vehicle's users can sell the extra electricity to grid management. These two bi-directional operation modes are controlled by both voltage regulator and current regulator. The operation of voltage regulator and current regulator also depends on the battery voltage and current due to various charging sequences adopted in the proposed system which is explained in more detail in Section IV.

3. Design of Coupled Inductor

The large ripple in battery charging current incurs stresses to a battery and eventually shortens the life time of battery. In order to reduce the filter inductor size, coupling of output inductors in two-phase interleaved dc-dc converters is employed. The circuit schematic and physical magnetic structure of coupled inductor is illustrated in Fig. 3 along with the actual photo in Fig. 4. The core structure has three legs of E-E core so that the coupling factor between two windings can be adjusted by the air gap distance in

the center leg. The coupling factor of negative 0.5, i.e. inverse coupling, is selected in the proposed system in order to minimize the peak current of individual inductor. This coupling factor of negative 0.5 has been obtained through theoretical modeling of coupling inductor and circuit simulation as explained in the following paragraphs.

In general, the inductor voltages of coupled inductor can be represented in terms of the self and mutual inductances as in (1) and (2). Flux linkage equations are written under the condition of direct coupling for the sake of general description.

$$V_{L\_BCU\_1} = \frac{d}{dt}(\lambda_{11} + \lambda_{21}) = L_{11}\frac{d}{dt}i_{L\_BCU\_1} + L_{21}\frac{d}{dt}i_{L\_BCU\_2} \quad (1)$$

$$V_{L\_BCU\_2} = \frac{d}{dt}(\lambda_{22} + \lambda_{12}) = L_{22}\frac{d}{dt}i_{L\_BCU\_2} + L_{12}\frac{d}{dt}i_{L\_BCU\_1} \quad (2)$$

In (1) and (2), L_{11} and L_{22} represent the self inductance terms while L_{12} and L_{21} represent the mutual inductance terms. Mutual inductances are equal to each other based on reciprocity property as shown in (3).

$$\frac{\lambda_{12}}{i_{L\_BCU\_1}} = \frac{\lambda_{21}}{i_{L\_BCU\_2}} = L_{12} = L_{21} = M \quad (3)$$

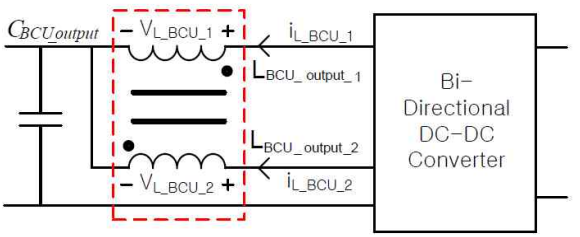

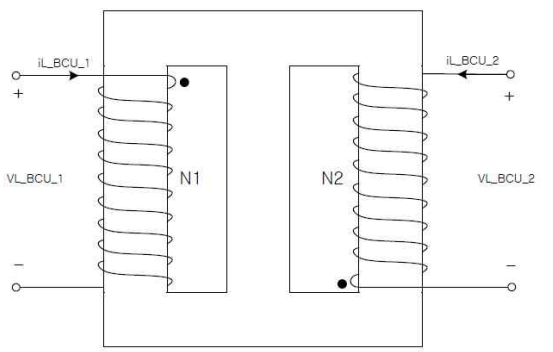

Fig. 3 Schematic and magnetic structure of coupled inductor employed in dc-dc converter

The coupling factor (α) is the key design factor in a coupled inductor and is defined in (4). Positive coupling factor refers to a direct coupling while negative number means an inverse coupling. The coupled inductor employed in this paper adopts the symmetric magnetic structure.

$$\alpha = \frac{M}{\sqrt{L_{11}L_{22}}}, L = L_{11} = L_{22} \quad (4)$$

Using (3) and (4), inductor voltage equations of (1) and (2) can be simplified to (5).

$$V_{L\_BCU\__1} - \alpha V_{L\_BCU\_2} = (1-\alpha^2)L_{11}\frac{d}{dt}i_{L\_BCU\_1} \quad (5)$$

Because of the coupling mechanism of inductor, two inductor voltages ($V_{L\_BCU\_1}$, $V_{L\_BCU\_2}$) are correlated to each other depending on the switching states of SW_{BCU_U1} and SW_{BCU_U2}. A total of three different combinations of switching states are possible.

$$\begin{cases} SW_{BCU\_U1} = on \\ SW_{BCU\_U2} = off \end{cases} \Rightarrow V_{L\_BCU\_2} = -\frac{D}{1-D}V_{L\_BCU\_1} \quad (6)$$

$$\begin{cases} SW_{BCU\_U1} = on \\ SW_{BCU\_U2} = on \end{cases} OR \begin{cases} SW_{BCU\_U1} = off \\ SW_{BCU\_U2} = off \end{cases} \quad (7)$$

$$\Rightarrow V_{L\_BCU\_2} = V_{L\_BCU\_1}$$

$$\begin{cases} SW_{BCU\_U1} = off \\ SW_{BCU\_U2} = on \end{cases} \Rightarrow V_{L\_BCU\_2} = -\frac{1-D}{D}V_{L\_BCU\_1} \quad (8)$$

Using one of three equations of (6), (7), and (8) depending on the switching state, the inductor voltage equation of (5) can be written as

$$V_{L\_BCU\_1} = L_{eq}\frac{d}{dt}i_{L\_BCU\_1} \quad (9)$$

where L_{eq} is expressed by one of the following three equations corresponding to the switching state. [16]

$$\begin{cases} SW_{BCU\_U1} = on \\ SW_{BCU\_U2} = off \end{cases} \Rightarrow L_{eq} = \frac{1-\alpha^2}{1+\frac{D}{1-D}\alpha}L \quad (10)$$

$$\begin{cases} SW_{BCU\_U1} = on(off) \\ SW_{BCU\_U2} = on(off) \end{cases} \Rightarrow L_{eq} = (1+\alpha)L \quad (11)$$

$$\begin{cases} SW_{BCU\_U1} = off \\ SW_{BCU\_U2} = on \end{cases} \Rightarrow L_{eq} = \frac{1-\alpha^2}{1+\frac{1-D}{D}\alpha} L \qquad (12)$$

As a result, the coupling inductor turns out to have a variable equivalent inductance (L_{eq}) depending on the corresponding time interval. This variable equivalent inductance can be either smaller or larger than self inductance (L_{11} and L_{22}) depending on the value of duty ratio (D) and coupling factor (α). In [16], the coupled inductor current has a smaller peak-to-peak ripple size than non-coupled case if inverse coupling is utilized under the condition of duty ratio lower than 0.5.

4. Control Algorithm of Lithum-Ion Polymer Battery Charging System

The control algorithm of battery charging operation in this paper has been designed to meet the long life-cycle and safe operating requirement of lithium-ion and lithium-polymer battery. During the charging state, the cell voltage should not exceed its end-of-charge voltage (about 4.1V/cell) to prevent over-charging and dissolving the copper in electrolyte which would damage the active materials of the lithium - ion and lithium-polymer cell. During the discharging state, the cell voltage also should not go below its low voltage threshold (about 2.7V/cell) to prevent over-discharge and damaging the cell capacity.

The proposed charging algorithm consists of three sub-interval charging sequences as shown in Fig. 5 and 6. If cell voltage is below the threshold voltage of 2.7V/cell, the charger gradually ramps up charging current to avoid damaging the battery. This charging sequence is called as Pre-charge Mode. The ramping up of charging current follows the stair-case like current reference waveform as illustrated in Fig. 6. As compared to conventional trickle mode charging pattern, this stair-case ramping up pattern does not involve pulsating charge current so that state-of-charge can be lifted above the level of pre-charge mode in a more smooth and reliable manner minimizing the stress to the battery.

When the cell voltage increases over the threshold voltage of 2.7V/cell, charging sequence moves to Constant Current (CC) Charging Mode. During CC mode, maximum current is supplied for rapid charging so that the charging time is maintained within about 16min to attain 80% state-of-charge. As the battery voltage reaches the end-of-charge voltage of 4.1V/cell, Constant Voltage (CV) Charging Mode is initiated to fully charge the battery maintaining the voltage at its end-of-charge voltage. In order to avoid

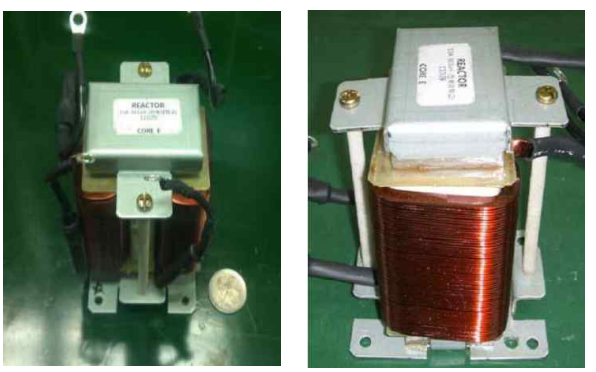

Fig. 4 Photo of coupled inductor used in the proto-type

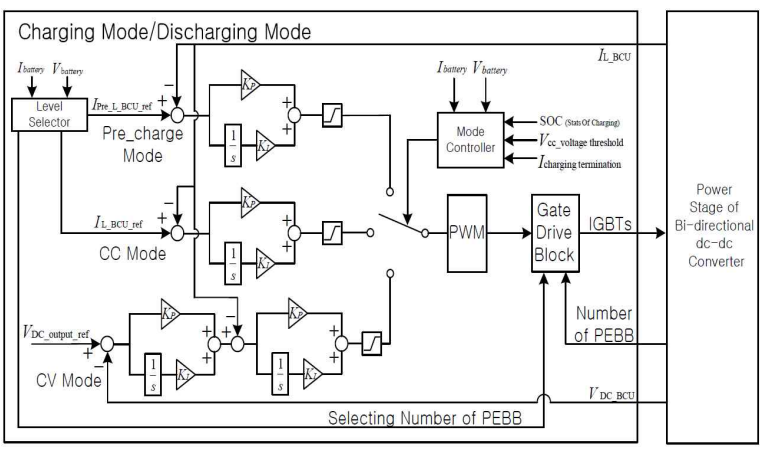

Fig. 5 Overall control block diagram of battery charging and discharging unit

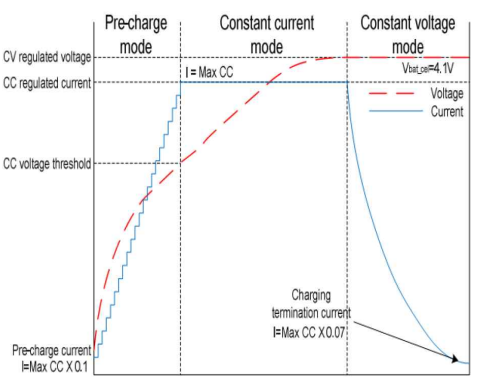

Fig. 6 Proposed charging profile of Li-Ion Polymer battery

Table 1 Specifications of Electric Vehicle Battery Charge System

Specification	Values	Specification	Values
Rated power	30kW	Pre-charge mode voltage	292V
AC input voltage	342~506V	Pre-charge mode current	0~78A
AC input current	77A	Constant voltage mode voltage	440V
DC-link voltage	858V	Constant current mode current	78A
DC output voltage	50~450V	Battery capacity	11.4kWh

over-charging the battery, CV mode is stopped when the charging current reaches the pre-defined termination current as illustrated in Fig. 6.

Pre-charge mode and CC mode involve current regulator of inductor current whose reference is determined depending on the measured battery voltage as shown in Fig. 5. During CV mode both of voltage regulator and current regulator are employed in the control algorithm. In Fig. 5 the voltage regulator is put in the outer loop to provide the current reference to inner current regulator, i.e. nested multiple control loop architecture.

5. System Verification

The proposed topology and control algorithm for a rapid charging system is verified through simulation and experiment on a laboratory proto-type. The operating condition for the simulation and experimental verification is specified in Table I. The rated power of complete charging system is set to 30kW. The range of input voltage without derating the output power is from 342V to 506V. This is aimed to meet both ac line nominal condition of 380V and 460V. The output voltage at the battery side of bi-directional dc-dc converter is designed to cover between 50V and 450V. This wide operating range makes it possible for the charger to effectively realize proposed charging sequences of the battery.

Simulation verification of the proposed system and its control algorithm has been performed using the power electronic circuit simulation tool of PLECS. Battery has been modeled based on the charging and discharging curve (Voltage vs. SOC) provided by a battery manufacturer. The operation of coupled inductor has been compared with non-coupled inductor case through the simulation. The phase-staggered inductor currents for the case of non-coupled inductor, i.e. zero coupling factor, are described in Fig. 7. The same waveforms for the case of coupled inductor having the inverse coupling factor of 0.5 are also given in Fig. 8. It is noted from Fig. 7 and 8 that the peak-to-peak ripple of individual inductor current is smaller for the case of coupled inductor than the case of non-coupled inductor as mentioned in Section III. However, at the down-stream of inductor, the added phase-staggered inductor current has the larger ripple size for the case of coupled inductor than that of non-coupled inductor. This is because the harmonic components generated by coupling effect, otherwise non-existing under the condition of non-coupled case, are added instead of subtracted by phase-staggering operation. Figure 9 describes the variation of peak-to-peak value of individual inductor current with respect to the coupling factor of a coupled inductor. It is noted from Fig. 9 that the coupling factor of 0.5 would lead to the smallest value of peak-to-peak individual inductor ripple current. Figure 10 describes the variation of peak-to-peak ripple value of summed inductor current with respect to the coupling factor under the condition of 3 BCU modules, i.e. 6-phase interleaved. It is noted from Fig. 10 that the coupling doesn't contribute in minimizing the ripple size of summed inductor current.

Although coupling the output inductor in phase-staggering operation doesn't necessarily lead to the smaller ripple size of battery charging current, the coupled inductor still has the advantage of smaller peak-to-peak individual inductor current and smaller core size as compared to the non-coupled case. In fact, phase-staggering operation itself greatly reduces the ripple size of battery charging current so that the negative impact of coupling the choke on the ripple size is hardly noticeable as shown by the absolute values of ripple size in Fig. 10. For example, the ripple size of summed inductor current at the coupling factor of 0.5 in Fig. 10 is approximately 5mA whose ripple factor is far less than 1% of 78A.

In order to verify the proposed charging algorithm in this paper, the complete charging sequence starting from pre-charge mode to final charge termination in CV mode has been simulated using the employed battery model. The waveforms of battery voltage and current during this complete charging sequence are plotted in Fig. 11. Because of the relatively long time

duration of CV mode, the time range of CV mode has been truncated to better describe the performance of all three charging modes. When battery voltage is below the threshold voltage of 292V, i.e. 2.7V/cell, EV rapid charging system operates under pre-charge mode. During this pre-charge mode, the battery current is increased in a step-wise pattern in order to slowly charge the battery up to the point where the full-strength charging of CC mode can be initiated.

When the battery voltage reaches the threshold voltage of 292V, then CC mode starts to supply the rated current of 26A per one BCU module, i.e. 78A for a complete battery stack. CC mode lasts until the battery voltage reaches the end-of-charge voltage of 440V (about 4.1 V/cell). During CC mode, maximum current of 78A for the case of three BCU modules is supplied for rapid charging so that the charging time is maintained within about 16 min to attain 80% state-of-charge. In order to prevent over-charging the battery, CV mode is executed to keep the voltage at its end-of-charge voltage of 440V. DC output battery voltage is shown to be maintained at 440V securing the safe margin of 10V against 450V of end-of-charge voltage. The complete charging sequence is finished when the battery charging current is decreased below the charging termination current of 1.6A as shown in Fig. 11. The laboratory proto-type of 30kW rapid charging system has been built and tested to verify the proposed concept in this paper. Figure 12 presents the full view of proto-type of rapid EV charger.

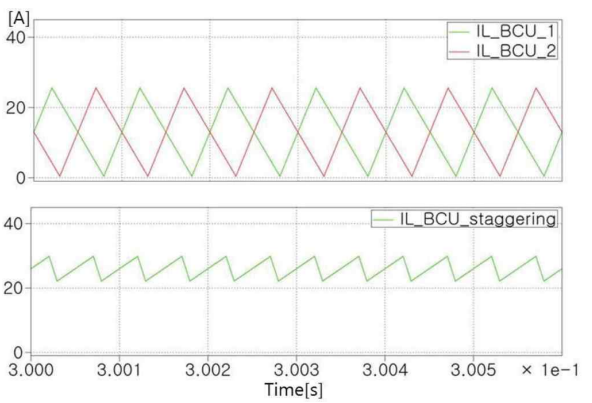

Fig. 7 Simulation waveforms of phase-staggered inductor currents in dc-dc converter employing a non-coupled inductor (Top: $I_{L\_BCU\_1}$, $I_{L\_BCU\_2}$, Bottom: $I_{L\_BCU\_staggering}$)

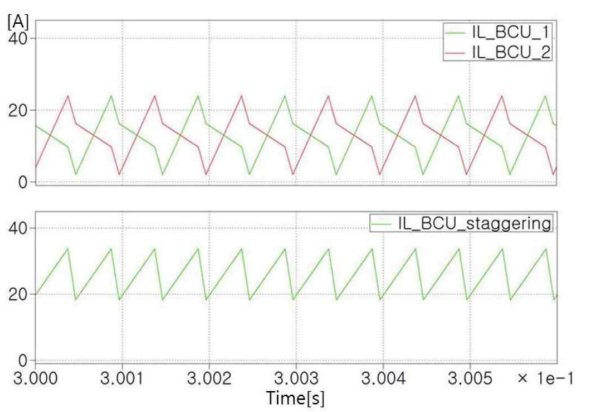

Fig. 8 Simulation waveforms of phase-staggered inductor currents in dc-dc converter employing a coupled inductor (Top: $I_{L\_BCU\_1}$, $I_{L\_BCU\_2}$, Bottom: $I_{L\_BCU\_staggering}$)

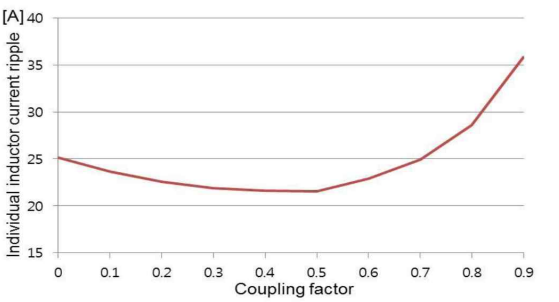

Fig. 9 Characteristic of peak-to-peak value of individual inductor current($I_{L\_BCU\_1}$) vs. coupling factor(α) of a coupled inductor

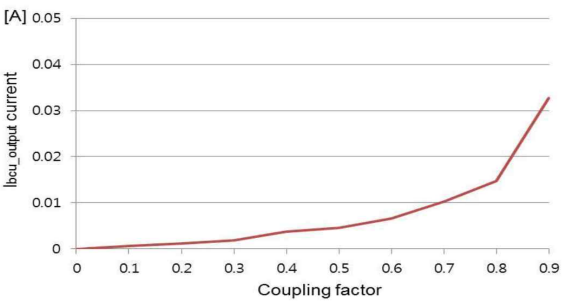

Fig. 10 Characteristic of peak-to-peak ripple value of summed inductor current (6 phase-staggered I_{DC_output}) vs. coupling factor(α) of a coupled inductor

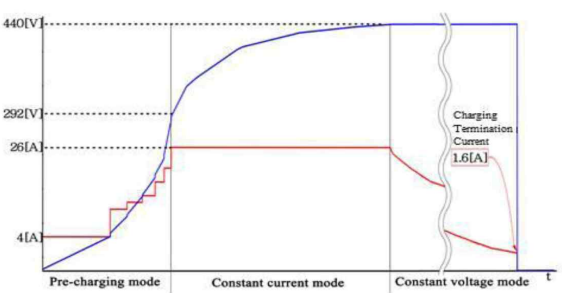

Fig. 11 Simulation waveform of charging voltage (V_{DC_output}) and current (I_{BCU_output}) from single BCU module during a complete charging sequence

The power stack of active front-end rectifier unit and battery charging/discharging unit are shown in Fig. 13. Coupled inductor design makes BCU structure more compact and module-friendly. Lithium-ion battery pack used for testing the proto-type charger is shown in Fig. 14.

Waveforms of three-phase ac input voltages and the dc link voltage under the input voltage of 460V are given in Fig. 15. As noted in Fig. 15, dc link voltage is well regulated to be 858V. AC input currents obtained under the condition of unity power factor are shown in Fig. 16. It is noted from Fig. 16 that the harmonic contents in ac input currents having THD of less than 5% comply with the requirement from IEEE 519-1992 under the condition of 10kHz switching frequency and the ac side total inductance of 12% including short-circuit impedance from the grid. Fig. 17 describes the transient behavior of ARU following a step change of ac line voltage from 460V to 380V.

Figure 18 and 19 illustrates the operation of dc-dc converter in BCU under constant current charge

Fig. 12 Rapid EV charger proto-type

Fig. 13 Power stack built for the proto-type

Fig. 14 Li-Ion polymer battery pack and electric vehicle used for testing the charger setup

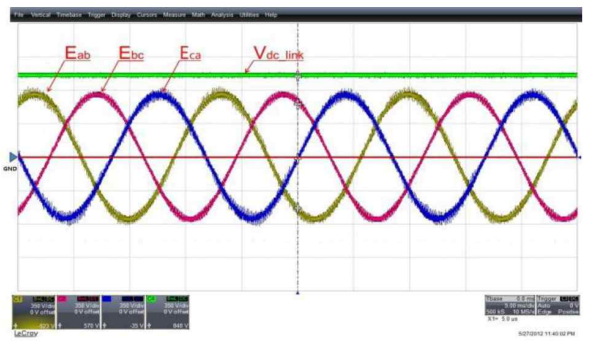

Fig. 15 Experiment waveforms of ac input voltages and dc link voltage of active rectifier unit under ac input of 460V
(E_{ab}, E_{bc}, E_{ca}, and V_{dc_link}[350V/div, 5ms/div])

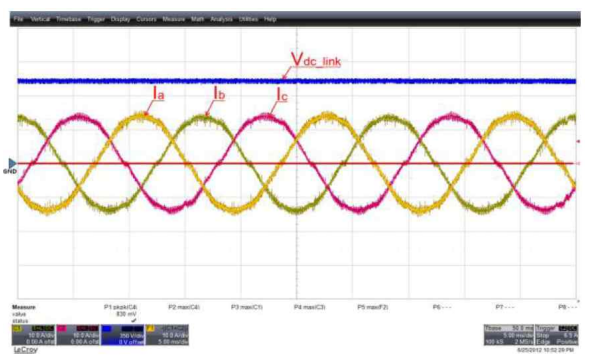

Fig. 16 Experiment waveforms of ac input currents and dc link voltage of active rectifier unit under ac input of 460V
(I_a, I_b, I_c[10A/div 5ms/div], and , V_{dc_link}[350V/div])

Fig. 17 Experiment waveforms of dc link transient response under ac line input drop by 18%
(E_{ab}, E_{bc}, E_{ca}, and V_{dc_link}[350V/div, 20ms/div])

mode. The output voltage of BCU which is same as the battery voltage is equal to 410V. The battery charging current of 17A is provided by dc-dc converter in BCU. Due to the limitation of test environment, the rated charging current of 78A during CC mode has been down-scaled to 17A. The battery voltage and cell voltage under the constant charging current of 12A is shown with respect to the States of Charge (SOC) in Fig. 20 and 21, respectively. In order to confirm the effective operation of BMS(Battery Management System) inside the battery pack, the maximum and minimum values of each cell voltage are also plotted in Fig. 21. Hardware test under rated condition is under progress and the result will be reported in future publications.

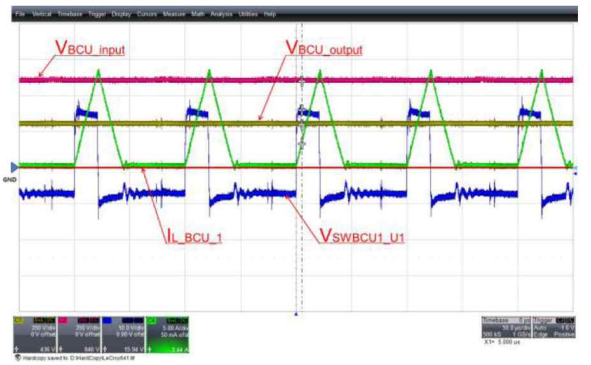

Fig. 18 Experiment waveforms of input & output voltage, inductor current, and switching gate voltage in the battery charging unit under Constant Current (CC) mode (V_{BCU_input}, V_{BCU_output}[350V/div, 50us/div], $I_{L\_BCU\_1}$[5A/div], and V_{swBCU1_U1}[10V/div])

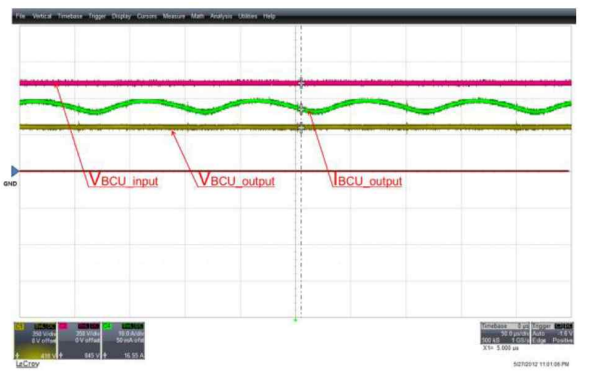

Fig. 19 Experiment waveforms of input & output voltage and battery charging current in the battery charging unit under Constant Current (CC) mode (V_{BCU_input},V_{BCU_output}[350V/div,50us/div],and I_{BCU_output}[10A/div])

6. Conclusion

This paper presents a simple and cost-effective rapid battery charging system of 30kW for electric vehicles. The proposed stand-alone off-line charging system mainly consists of active front-end rectifier of neutral point clamped 3-level type and non-isolated bi-directional dc-dc converter of multi-phase interleaved half-bridge topology. The charging system is designed to operate for both lithium-polymer and lithium-ion batteries. The complete charging sequence is made up of three sub-interval operating modes; pre-charge mode, constant-current mode, and constant-voltage mode. The pre-charge mode employs the stair-case shaped current profile to accomplish shorter charging time while maintaining the reliable operation of the battery. The proposed charge system is specified to reach the full-charge state within less than 16min for the battery capacity of 8kWh by supplying the charging current of 78A. This proposed charging sequence is set to meet the long life-cycle and safe operating requirement of the battery.

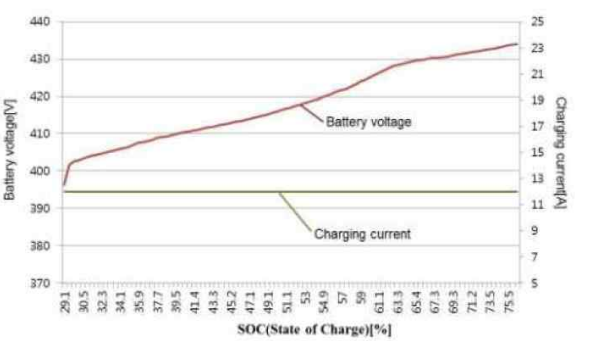

Fig. 20 Characteristic of battery charging current (I_{DC_output}) and battery voltage (V_{DC_output}) vs. State of Charge (SOC) under Constant Current (CC) charging mode

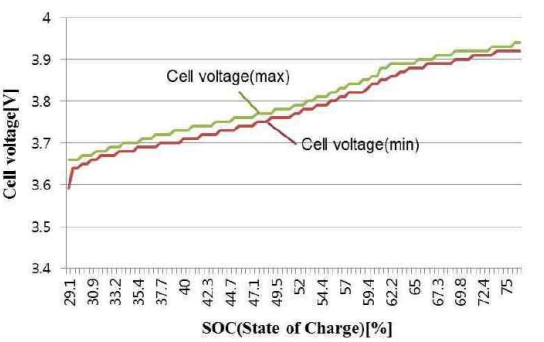

Fig. 21 Characteristic of maximum and minimum battery cell voltage vs. State of Charge (SOC) under Constant Current (CC) charging mode

The charging time less than 16min is made possible by the improved current capability of the battery and the cost-effective PEBB structure of charging unit.

The proposed charging system in this paper is equipped with a line-frequency transformer for galvanic isolation at the ac input side of system. Despite of its weight and volume, this low-frequency transformer has the cutting-edge advantage of low cost and simple interface in a separate off-line charging station as compared to high-frequency transformer generally employed for isolated bi-directional dc-dc converters. Owing to the simple and compact power conversion scheme, the proposed solution has superior module-friendly mechanical structure which is absolutely required to realize flexible power expansion capability in a very high-current rapid charging system. The simulation and experiment results confirm the unique features of the proposed system and its control algorithm. The phase-staggering operation of all three modules in the battery charging unit is under test and the corresponding result will be reported in future publications.

This work was supported by the Smart Grid Research Center at Chonbuk National University in Korea.

References

[1] M. Bojrup, P. Karlsson, M. Alakula, and B. Simonsson, "A dual purpose battery charger for electric vehicles," in *IEEE Power Electronics Specialists Conference*, Vol. 1, pp. 565-570, 1998.

[2] D. Aggeler, F. Canales, H. Zelaya-De La Parra, A. Coccia, N. Butcher, and O.Apeldoorn, "Ultra-fast dc-charge infra structures for EV-mobility and future smart grids," in *IEEE Innovative Smart Grid Technologies Conference*, pp. 1-8, 2010.

[3] C. C. Chan and K. T. Chau, "An overview of power electronics in electric vehicles," in *IEEE Trans. Ind.* Appl., Vol. 44, No. 1, pp. 3-13, Feb. 1997.

[4] S. G. Wirasingha, N. Schofield, and A. Emadi, "Plug-in hybrid electric vehicle developments in the US: Trends, barriers, and economic feasibility,"in *IEEE 2008 Vehicle Power and Propulsion Conference*, pp. 1-8, 2008.

[5] S. Haghbin, K. Khan, S. Lundmark, M. Alakula, O. Carlson, M. Leksell, and O. Wallmark, "Integrated chargers for EV's and PHEV's: examples and new solutions," in *ICEM 2010 XIX International Conference*, pp. 1-6, 2010.

[6] L. Solero, "Nonconventional on-board charger for electric vehicle propulsion batteries," in *IEEE Trans. Vehicular Technology*, Vol. 50, pp. 144, Jan. 2001.

[7] D. Yu, Z. Xiaohu, B. Sanzhong, S. Lukic, and A. Huang, "Review of non-isolated bi-directional DC-DC converters for plug-in hybrid electric vehicle charge station application at municipal parking decks," in *IEEE 2010 Applied Power Electronics Conference and Exposition*, pp. 1145, 2010.

[8] D. Yu, Z. Xiaohu, B. Sanzhong, S. Lukic, and A. Huang, "Review of non-isolated bi-directional DC-DC converters for plug-in hybrid electric vehicle charge station application at municipal parking decks," in *IEEE 2010 Applied Power Electronics Conference and Exposition*, pp. 1145, 2010.

[9] H. Sangtaek and D. Divan, "Bi-directional dc/dc converters for plug-in hybrid electric vehicle (PHEV) applications," in *IEEE 2008 Applied Power Electronics Conference and Exposition*, pp. 784-789, 2008

[10] K. W. Klontz, A. Esser, P. J. Wolfs, and D. M. Divan, "Converter selection for electric vehicle charger systems with a high-frequency high-power link," in *IEEE 1993 Power Electronics Specialists Conference*, pp. 855-861, 1993.

[11] M. Ortúzar, J. Dixon, and J. Moreno, "Ultra capacitor based auxiliary energy system for an electric vehicle: Implementation and evaluation," in *IEEE Trans. Ind. Electron.*, Vol. 54, No. 4, pp. 2147-2156, Aug. 2007.

[12] R. M. Schupbachj and C. Bald, "Comparing dc-dc converters for power management in hybrid electric vehicles," in *IEEE 2003 International Electric Machines and Drives Conference*, Vol. 3, pp. 1369-1374, 2003.

[13] J. Czogalla, J. Li, and C. R. Sullivan, "Automotive application of multi-phase coupled-inductor dc-dc converter," in *IEEE Industry Applications Conference*, Vol. 3, pp. 1524-1529, 2003.

[14] M. Gerber, J. A. Ferreira, N. Seliger, and I. W. Hofsajer, "Design and evaluation of an automotive integrated system module," in *IEEE Industry Applications Conference*, Vol. 2, pp. 1144-1151, 2005.

[15] Y. Suh, Y. Go, and D. Rho "A comparative study on control algorithm for active front-end rectifier of large motor drives under unbalanced input," in *IEEE Trans. Ind. Appl.*, Vol. 47, No. 3, pp. 1419-1431, May/June 2011.

[16] P-L. Wong, P. Xu, B. Yang, and F. C. Lee, "Performance improvements of interleaving VRMs with coupling inductors," in *IEEE Trans. Power Electron.*, Vol. 16, No. 4, pp. 499-507, July 2001.

[17] M. C. Kisacikoglu, B. Ozpineci, and L. M. Tolbert, "Reactive power operation analysis of a single-phase EV/PHEV bidirectional battery charger," in *IEEE International Conference Power Electronics-ECCE Asia*, pp. 585-592, May 2011.

Taewon Kang was born in Jeonju, Korea. He received his B.E.E. and M.S.E.E. from Chonbuk National University, Jeonju, Korea in 2010 and 2013, respectively, where he is currently working toward the Ph.D. degree. His research interests include electric drivers, power devices, and power converters for renewable energy sources.

Yongsug Suh was born in Seoul, Korea. He received his B.E.E. and M.S.E.E. from Yonsei University, Seoul, Korea, in 1991 and 1993, respectively, and his Ph.D. in Electrical Engineering from the University of Wisconsin, Madison, in 2004. From 1993 to 1998, he was an Application Engineer in the Power Semiconductor Division of Samsung Electronics Co. From 2004 to 2008, he was a Senior Engineer in the Power Electronics & Medium Voltage Drives Division of ABB, Turgi, Switzerland. Since 2008, he has been with the Department of Electrical Engineering, Chonbuk National University, Jeonju, Korea, where he is currently an Associate Professor. His research interests include power conversion systems of high power for renewable energy sources and medium voltage electric drive systems.

Hyeoncheol Park was born in Iksan, Korea. He received his B.E.E. and M.S.E.E. degree from Chonbuk National University, Jeonju, Korea in 2008 and 2011 respectively. since 2011 he has been working for Iljin electric Co. His research interests include electric drives, power devices, and power converters for renewable energy sources and environment -friendly energy conversion systems.

Byungik Kang was born in Seoul, Korea. He received his B.E.E. degree from Kwangwoon University, Seoul, Korea in 2008. Since 2009 he has been working for Iljin electric Co. His research interests include electric vehicle and PHEV, rapid charging system and ESS.

Simon Kim as born in Seoul, Korea. He received his M.S.E.E. from Brown University, Rhode Island, USA, and his Ph.D. in University of Ohio, Athens. He was an Iljin holdings Co. and he has been a Director of next generation technology research team in Iljin Co. His research interests include power conversion systems of high power for renewable energy sources and ESS, LIB, and Battery charging system for EV.